# Combined Kinetic and Bean-Rodbell approach for describing field-induced transitions in LaFe$_{11.6}$Si$_{1.4}$ alloys

L. M. Moreno-Ramírez [a], J. S. Blázquez [a], I. A. Radulov [b], K. P. Skokov [b], O. Gutfleisch [b], V. Franco * [a] and A. Conde [a]

[a] *Dpto. Física de la Materia Condensada, ICMSE-CSIC, Universidad de Sevilla, P.O. Box 1065, 41080-Sevilla, Spain*

[b] *Institut für Materialwissenschaft, TU Darmstadt, 64287 Darmstadt, Germany*

*Corresponding author: V. Franco, vfranco@us.es

## Abstract

We propose a combination of the Kolmogorov-Johnson-Mehl-Avrami nucleation and growth theory and the Bean-Rodbell model to describe the field-induced transition in LaFe$_{11.6}$Si$_{1.4}$ alloys. The approach is applied to a set of bulk samples undergoing first-order transitions produced by different routes and including doping effects. The kinetic analysis of both magnetization and demagnetization processes reveals a nucleation and three-dimensional interface-controlled growth for these alloys. Introducing the kinetic process between the metastable and stable solutions of the Bean-Rodbell model, the field dependence of the magnetization/demagnetization processes, including magnetic hysteresis for different magnetic field sweeping rates, is better reproduced than with the pure model.

## 1. Introduction

Hysteresis phenomena deserve the attention of the magnetocaloric (MC) research community since the discovery of giant effects associated to first-order transitions of magnetic materials [1]. The possibility of using these materials for cooling applications are related with the associated hysteresis, being low hysteretic materials (among other aspects) highly desired for applications [1-4]. La(Fe,Si)$_{13}$ alloys are among the most promising families of MC materials as they exhibit a high MC response with relatively small hysteresis that can be tuned by hydrogenation up to room temperature [5-7]. Experimentally, different routes have been proposed for minimizing the hysteresis of MC materials [8] as element doping [9], structural modifications [10] or the use of external loads [11, 12].

For a better understanding of the different sources of hysteresis, it is important to find procedures to describe and model the thermomagnetic transitions [13, 14]. In the case of La(Fe,Si)$_{13}$ alloys, the MC response is ascribed to an itinerant-electron metamagnetic transition from the para (PM) to the ferromagnetic (FM) state with a relatively small volume change ($\approx$ 1 %) without modification of the crystal structure (i.e. a magnetoelastic transition). This type of transitions can be modeled by the Bean-Rodbell model [15]. Although this model was originally developed in the framework of localized magnetic moment, it can be successfully extended to electron itinerant systems such as La(Fe,Si)$_{13}$ alloys by considering that the magnetic moment arises from the unpaired electrons of the 3d-4s band [16-18]. Although the Bean-Rodbell model qualitatively illustrates the magnetic behavior of La(Fe,Si)$_{13}$ materials, two main issues have to be considered: 1) the predicted hysteresis values are larger than the experimentally observed ones and 2) the extremely abrupt drop of the magnetization at the transition is also in disagreement with experimental data [13,19-21]. Moreover, the experimental hysteresis phenomena have been shown to depend on different characteristics (e.g. sweep rate, shape, surface etc [8, 22-24]) which are not considered in the model.

To solve these issues and incorporate new characteristics, we introduce the idea of a kinetic process into the thermomagnetic model. The classical nucleation and growth theory of Kolmogorov-Johnson-Mehl-Avrami (KJMA) [25-29] has been selected in this work as the kinetic part to be incorporated into the Bean-Rodbell description. By combining both Bean-Rodbell model and KJMA theory, we

successfully describe the field dependence when magnetizing and demagnetizing for a set of LaFe$_{11.6}$Si$_{1.4}$ samples with different characteristics (doping effects and different synthesis routes). Using the proposed combination the hysteresis is described in detail for different magnetic field sweeping rates while using the pure Bean-Rodbell model significantly overestimated values are obtained (up to 200 % for the studied cases).

## 2. Models

### 2.1. Bean-Rodbell model

This Bean-Rodbell model assumes that the relative volume change ($w$) affects the transition temperature ($T_t$) according to:

$$T_t = T_0(1 + \beta w) \tag{1}$$

where $T_0$ is the transition temperature in absence of volume changes and $\beta$ an introduced parameter. According to this model, the magnetization ($M$) is obtained as (see the mathematical appendix of the supplementary material and ref. [30] for a detailed introduction to the model):

$$\frac{M}{M_S} = B_J\left(\frac{g\mu_B J}{k_B T}\mu_0 H + \frac{3T_0}{T}\left(\frac{J}{J+1}\right)\frac{M}{M_S} + \eta\frac{9}{10}\left(\frac{2J^2 + 2J + 1}{(J+1)^3}\right)\frac{T_0}{T}\frac{M^3}{M_S{}^3}\right), \tag{2}$$

where $M_S$ is the saturation magnetization, $B_J$ the Brillouin function, $g$ the Landé factor, $\mu_B$ the Bohr magneton, $J$ the total quantum angular momentum, $\mu_0$ the vacuum permeability, $H$ the magnetic field and $\eta$ the order parameter of the model, defined as:

$$\eta = \frac{5}{2}\left(\frac{(2J+1)^4 - 1}{(2(J+1))^4}\right)\frac{M_S}{g\mu_B J}k_B T_0 k\beta^2, \tag{3}$$

where $k$ is the compressibility. The $\eta$ parameter controls the order of the transition, being of first-order if $\eta > 1$, second-order if $\eta < 1$ and $\eta = 1$ corresponds to the critical point (where the order of the transition changes from second to first). $T$ has a single-valued solution as a function of $M$ and $H$ in **eq. (2)**. For $\eta > 1$, metastable and instable regions appear in the solution [31]. The stable solution (with a critical field $H_c^{st}$) is obtained when the energy of FM and PM phases is the same, which is calculated according to the so-called equal-area construction from the single-valued solution (making the area below the

metastable and instable branches equal for both phases) [32]. The existence of the metastable branches leads to two different solutions when the material is magnetized or demagnetized (with different critical fields $H_c^m$ and $H_c^d$, respectively, which are not the same as the stable solution), which gives rise to associated hysteresis. All this features are illustrated in **Fig. 1 (a)**.

### 2.2. KJMA theory

Nucleation and growth kinetic theories has been previously used in first-order magnetocaloric materials including La(Fe,Si)$_{13}$ alloys [33-35]. However, the interpretation is not clear, as the kinetic effect can be promoted by local heating/cooling at the phase boundary due to the magnetocaloric temperature change of the material, due to dipole interactions between moments or by thermal activation over an energy barrier. Nevertheless, these possible origins of the kinetic effect, which depend on the specific material, do not modify the framework that we propose.

In KJMA theory the isothermal transformed fraction ($X$) as a function of time ($t$) is expressed as:

$$X(t) = 1 - e^{-K(t-t_0)^n}, \tag{4}$$

where $K$ (frequency factor) and $n$ (Avrami exponent) are the model parameters and $t_0$ is the induction time for which the transformation starts. The value of the Avrami exponent is related to the nucleation and growth mechanisms of the transition. It can be expressed as $n = n_n + d \cdot n_g$ where i) $n_n$ is 1 for constant nucleation rate and 0 for absence of nucleation, ii) $d$ indicates the dimensions of the growth process (being 3 for a 3-d growth), and iii) $n_g$ is 1 for interface controlled growth or ½ for diffusion controlled growth [36]. For analyzing the field-induced transition, we need to correlate the time evolution of the transition to the driving force that produces it. Assuming that the system is in isothermal conditions and that the time required for the onset of the thermally activated transformation is larger than the one required to reach the field induced transformation, in a first approximation, time can be replaced by magnetic field in **eq. (4)** when the rate of field change ($\gamma$) is constant:

$$X(H) = 1 - e^{-L(H-H_0)^n},\tag{5}$$

being $L = K\gamma^{-1}$ and $H_0$ (i.e. $H(t_0)$) the magnetic field for which the transformation starts. This is a simplified expression in which we have neglected the field and temperature dependence of $L$ during the field variations [10]. Moreover, it should be noted that, apart from field and temperature, this transitions can also be driven by time [22]. In this first approximation for field-induced transitions, it has been assumed that the field evolution is fast enough to be the main responsible of the transition.

### 2.3. Proposed combination

Under the previously described assumptions we introduce KJMA theory in the Bean-Rodbell model for describing the magnetization as:

$$M = XM^{stable} + (1-X)M^{metastable},\tag{6}$$

where the magnetization superscript refers to the different solutions of the Bean-Rodbell model and $X$ is in the KJMA framework. It should be mention that for the magnetization/demagnetization process $X$ represents the fraction of FM/PM phase. The nexus between both models is that the magnetic field for which the transformation starts, $H_0$, should be the same as the critical field obtained by the model for the stable solution $H_c^{st}$. This is not imposed in our model, but will become an internal check of the validity of our approach, providing falsifiability to the model. With this, we are considering that the metastable phase is promoted to the stable one, starting from the critical field, by a nucleation and growth process as expected from the behavior of a first-order transition in which the two phases coexist during the transformation. This argument is valid for pure materials; if the material presents compositional inhomogeneities this condition can be relaxed. **Fig. 1 (b)** illustrates the proposed combined approach using different values of the $L$ factor and fixing $n = 4$ (as example).

## 3. Experimental

To check the reliability of the proposed model, first, we chose 1) a polycrystalline LaFe$_{11.6}$Si$_{1.4}$ sample synthetized by induction melting and subsequent suction casting and annealed 48 h at 1100 ºC [37], which presents a notable first-order

character. To extend the analysis, we also consider 2) a $LaFe_{11.4}Cr_{0.2}Si_{1.4}$ doped sample produced by the same synthesis procedures and 3) a $LaFe_{11.6}Si_{1.4}$ sample produced differently by induction melting and annealed for 10 days, with needle shape and measured at different field sweep rates. All these samples present very minor traces of α-Fe and LaFeSi phase (more significant in the case of sample 3) and good compositional homogeneity. Experimental values of the field dependences of magnetization close to the transition temperature region are measured using the vibrating sample magnetometer option in a Quantum Design PPMS. The direction of the magnetic field was applied in order to reduce the demagnetizing field on the sample (along the plate for suction casted samples and along the long direction of the needle for the induction melted sample), neglecting the demagnetizing factor of the sample piece in the analysis. Field sweep rate was 50 Oe/s for sample 1, 100 Oe/s for sample 2 and ranged from 10 to 100 Oe/s for sample 3.

## 4. Results and discussion

First, we focus on the suction casted $LaFe_{11.6}Si_{1.4}$ sample for a detailed description. The first step to model the field-induced transition (according to **eq. (6)**) is to determine the KJMA parameters (i.e. $n$, $L$ and $H_0$ of **eq. (5)**). For that, the transformed fractions have been calculated from the $M(H)$ curves assuming a linear behavior for the PM phase and a law of approach to saturation [38] for the FM phase (an example is shown in the Fig. S1 of the supplementary material). It should be noted that this procedure is general and independent of the Bean-Rodbell model. Moreover, the kinetic parameters can be obtained from other techniques without affecting the proposed combination (traditionally, calorimetry is widely employed; however, for field-induced transitions, that technique is not conventional and it is only available at a few research groups). After some algebra, **eq. (5)** can be transformed into (see mathematical appendix of the supplementary material):

$$H = H_0 + \frac{1}{L^{1/n}}(-\ln(1-X))^{1/n}. \tag{7}$$

This allows us to obtain $L$ and $H_0$ from the linear fit of $H$ vs. $(-\ln(1-X))^{1/n}$, by assuming a fixed value for $n$ (instead of using the conventional $\ln(-\ln(1-X))$

vs. $\ln(H - H_0)$ plot to obtain it [39]). The different possible values of exponent $n$ are those expected from a three dimensional growth (as the cell is cubic and there is no preferential directions) and are related to the different processes as summarized in **Table 1** [36].

In the framework of the KJMA model, values of $n$ larger than 4 do not correspond to any process with physical meaning and, therefore, these values are not considered. The different $H$ vs. $(-\ln(1-X))^{1/n}$ linear fits of the experimental data at 192 K during the magnetization and demagnetization processes are shown in **Fig. 2 (a)** and **(b)**, respectively. We exclude from the analysis the values corresponding to transformed fractions below 0.1 and above 0.9 due to the large relative error, as it is usual in the analysis of phase transformations using KJMA. From the results, it can be inferred that the best fittings are obtained when the Avrami exponent is equal to 4 (while the worst fitting corresponds to the lowest value of the Avrami exponent, $n$=1.5). According to the characteristics of these thermomagnetic transitions, $n$=4 is the most reasonable one because quenched-in nuclei are not expected in the reversible region and the transformation does not imply diffusion as structure and composition is preserved. Moreover, for $n$=4 the $H_0$ values during the magnetization and demagnetization processes are very similar, shown in **Fig. 2 (c)**, as it is expected as both metastable branches of the Bean-Rodbell model (for FM or PM phases) starts at the same critical field (see **Fig. 1 (a)**), reinforcing the election of $n$=4. These results show that $n$ is very sensitive to $H_0$ and that can lead to values of $n$ lower than expected (e.g. by using the $\ln(-\ln((1-X)))$ vs. $\ln(H - H_0))$ fitting) and could be ascribed to an "unexpected" two dimensional growth [33, 34].

However, though a good linear fit is obtained for the magnetization process, for the demagnetization case the fittings are significantly worse (as it can be observed from the values of the square of the sample correlation coefficient, $r^2$, being much better for the magnetization as the values are closer to 1), which illustrates the asymmetry of the transformation. **Fig. 3** shows the $H$ vs. $(-\ln(1-X))^{1/n}$ behavior for three isothermal demagnetization curves. It can be clearly observed that the process can be better described using two different slopes: one with a larger slope for low transformed fractions and another with

lower slope for high transformed fractions. It is worth mentioning that the values of the slope are inversely proportional to the value of $L$ (as it can be inferred from **eq. (7)**). The obtained values of the different kinetic parameters are shown in **Table 2**. We can see that the kinetic parameters are not significantly affected by the temperature, being in agreement with one of our initial assumption to neglect the temperature evolution during the magnetization process if isothermal conditions are not fulfilled. To show that the double slope procedure is not needed for the magnetization process, the $H$ vs. $(-\ln(1-X))^{1/n}$ behavior at 192 K at 50 Oe/s is shown in the inset of **Fig 3**. From **Table 2**, it can be observed that the demagnetization values of $L$ are smaller than those of the magnetization process (in the whole process), indicating a slower/more difficult transformation of the former with respect to the second one (contributing significantly to the hysteresis). The values obtained are going to be dependent on the sweeping field rate, so these values are valid only for 50 Oe/s (although they can be easily extended to other rates according to $L = K\gamma^{-1}$). For all the cases, the change of the slope is produced for a transformed fraction close to 0.4. This reveals that when the FM to PM transformation starts, it develops up to the 40 % of completion with much slower kinetics than that of the PM to FM transformation (a large slope corresponds to a small value of $L$). After that, the transformation rate increases up to completion (reaching values more similar to those of the PM to FM transformation). These features can be ascribed to the magnetic influence of the FM phase onto the PM one, being the transformation more favored as the FM fractions becomes less significant (although further studies are needed for clarifying this). However, it should be noted that either using one or two slopes provides a good agreement for magnetization results.

Once the kinetic parameters have been determined (i.e. $n$, $L$ and $H_0$), they have been introduced into the Bean-Rodbell model according to **eq. (5)**. The modeled magnetization curves are shown in **Fig. 4 (a)** together with the pure Bean-Rodbell model and the experimental data at 192 K and 50 Oe/s. To obtain the values of the different parameters of Bean-Rodbell model we fit the reversible low and high field regions of the $M(H)$ curves. It should be noted that, as we are fitting regions out of the transition, the obtained parameters are not going to depend on any factor that would modify the transformation (e.g. the sweeping rate). Fixing $g$=2,

$J$=1/2 (as the magnetic moment is ascribed to electrons) and $k = 8.6 \cdot 10^{-12}$ Pa$^{-1}$, the obtained values are $T_0$=185.7 K, $M_S$=1.29 $\cdot 10^6$ A/m and $\beta$=18.6 ($\eta$=1.59), which are similar to those found in the literature [40]. An excellent agreement between the modeled and experimental data is observed. The critical magnetic field of the stable solution (1.08 T) is quite similar to the $H_0$ found previously for both magnetization and demagnetization processes (see **Table 2**). This agreement serves as an internal validation of the proposed model. An additional validation consists in the fact that the transformation region in the JMAK model does not extend to fields beyond the metastable limits ($H_c^m$ and $H_c^d$) of the Bean-Rodbell model. From the experimental data together with the equilibrium solution, it is now clearly visible how the demagnetization process (the FM to PM transformation) is the main source of hysteresis of the material, as the transformation during magnetization occurs closer to the stable critical field of the Bean-Rodbell model, while demagnetization is more shifted to lower fields. This is in agreement with the conclusions extracted from the kinetic analysis, which shows a much slower rate of the FM to PM transformation at low transformed fractions (below $\approx$ 0.4). One of the main advantages of the proposed model is that the hysteresis is obtained with an excellent agreement, in contrast with the pure Bean-Rodbell model for which an overestimated value is obtained (1.2 T vs the experimental value of 0.4 T) as just the metastable limit (extremely fast measurements) is considered. This large hysteresis would correspond to an extremely fast transformation but delayed in field to the metastable limits in the proposed approach. Moreover, the evolution of magnetization during the transition is not reduced to an artificially abrupt change like in the pure Bean-Rodbell approach. To show the reproducibility of the procedure, we performed the same analysis for other isothermal curves at 190 and 194 K at 50 Oe/s, as shown in **Fig. 4 (b)**. To obtain a good fitting, the previously used parameters have been slightly modified, $T_0$ [from 184.6 to 186.7, i.e. a difference close to 1 %] and $\beta$ [from 18.5 to 18.7, i.e. a difference close to 1 %]. These very minor changes are expected as we are using a phenomenological model like Bean-Rodbell model as the basis for describing experimental data with good precision (e.g for a better description of the pressure dependence, new terms need to be introduced into the model [17]). The results show again a good agreement between the modeled data and the experimental ones, successfully describing the

hysteresis of the material. The critical field of the stable solution of the Bean-Rodbell model (0.65 and 1.51 T at 190 and 194 K, respectively) are again very similar to those of $H_0$ obtained by the kinetic analysis (see **Table 2**), validating our combined approach.

To further generalize the validity of our approach and check the influence of synthesis procedures, compositional effects and sweeping field rate, we have also studied two samples with compositional and synthesis differences: suction casted $LaFe_{11.4}Cr_{0.2}Si_{1.4}$ and induction melted $LaFe_{11.6}Si_{1.4}$. Performing a similar kinetic analysis as above, the kinetic parameters are obtained (the Avrami exponent is kept to 4). **Fig. 4 (c)** shows field dependence of the magnetization at 50 Oe/s and 186 K for the suction casted $LaFe_{11.4}Cr_{0.2}Si_{1.4}$, which shows stronger first-order character than previous sample. It can be observed, as previously, that the introduction of the kinetic process is fundamental for a better description of the hysteresis than using the pure Bean-Rodbell model. The fitted kinetic parameters are $L = 210$ and $130$ T$^{-4}$ (using a single slope this time for simplification) for the magnetization and demagnetization processes, respectively, obtaining, as previously, a slower kinetic process for the demagnetization than for the magnetization one. The use of just one single slope fitting for the demagnetization process is justified by the excellent agreement between modeled and experimental data (shown in **Fig. 4 (c)**). For this Cr-doped sample, the $L$ values (of both magnetization and demagnetization processes) are lower than those of the previous no Cr-doped sample. This is due the larger hysteresis for the Cr-doped sample with respect to the no Cr-doped sample, which makes the transformations further from the stable values and then reducing the $L$ values (this effect is illustrated in **Fig. 1 (c)**). The magnetic parameters are $T_0$=179.05 K, $M_S$=1.21·10$^6$ A/m and $\beta$=20 ($\eta$=1.68). **Fig. 4 (d)** shows field dependence of the magnetization at 100 and 10 Oe/s and 199 K for the induction melted $LaFe_{11.6}Si_{1.4}$, which shows weaker first-order character than previous sample. Due to the few experimental points at the transitions, the kinetic factor $L$ is affected by larger uncertainty. It has been obtained that $L$ is approximately 1.5·10$^3$ and 1.0·10$^3$ T$^{-4}$ for the magnetization and demagnetization at 100 Oe/s (these values are similar to those of the suction casted alloy with same composition). A good agreement between experimental and modeled results is

obtained at that rate. The magnetic parameters are $T_0$=195.94 K, $M_S$=1.34·10⁶ A/m and $\beta$=16.5 ($\eta$=1.37). In the case of 10 Oe/s, $L$ is obtained through the relation $L\left(10\ \frac{Oe}{s}\right) = 10 \cdot L\left(100\ \frac{Oe}{s}\right)$ (according to the approximations used to reach **eq. (5)**). At this low rate, the hysteresis is qualitatively well reproduced, however, an extra hysteresis phenomenon is observed (appearing at lower fields that expected). This can be ascribed, as previously mentioned, to extra effects (time or temperature induced) which are more relevant at such slow rates. For a finer reproducibility at lower rates a more general kinetic approach should be used, incorporating the different origins of the transformation.

## 5. Conclusions

We propose the combination of the Bean-Rodbell model and the KJMA theory to accurately describe the field-induced transition of bulk LaFe₁₁.₆Si₁.₄ first-order magnetocaloric alloys. Analyzing the kinetic behavior for different nucleation and growth processes, it has been found that both magnetization and demagnetization can be properly described using an Avrami exponent of 4, which is the one ascribed to a nucleation and three dimensional interface controlled growth. Combining these kinetic features with the stable and metastable solutions of the Bean-Rodbell model, we successfully describe the field dependence of the magnetization and demagnetization processes at different magnetic field sweeping rates for a set of samples with different characteristics (doping effects and different synthesis routes). Using the pure Bean-Rodbell model, the hysteresis is notably overestimated (up to 200 % for the studied cases). The existing asymmetry between magnetization and demagnetization processes is clearly reproduced, being the ferromagnetic to paramagnetic transformation a more relevant source of the hysteresis in comparison to the paramagnetic to ferromagnetic transformation.

## Tables

**Table 1.** Possibles values of the Avrami exponent ($n$) according to the different nucleation and growth characteristics of the transformation [36].

| $n_n$ | | $n_g$ | | $n = n_n + 3n_g$ (for a 3-d growth) |
|---|---|---|---|---|
| Constant nucleation | No nucleation | Diffusion growth | Interfacial growth | |
| - | 0 | ½ | - | 1.5 |
| 1 | - | ½ | - | 2.5 |
| - | 0 | - | 1 | 3 |
| 1 | - | - | 1 | 4 |

**Table 2.** KJMA parameters obtained from the $H$ vs. $(-\ln(1-X))^{1/4}$ fitting of the experimental data for the suction casted $LaFe_{11.6}Si_{1.4}$ sample at 50 Oe/s.

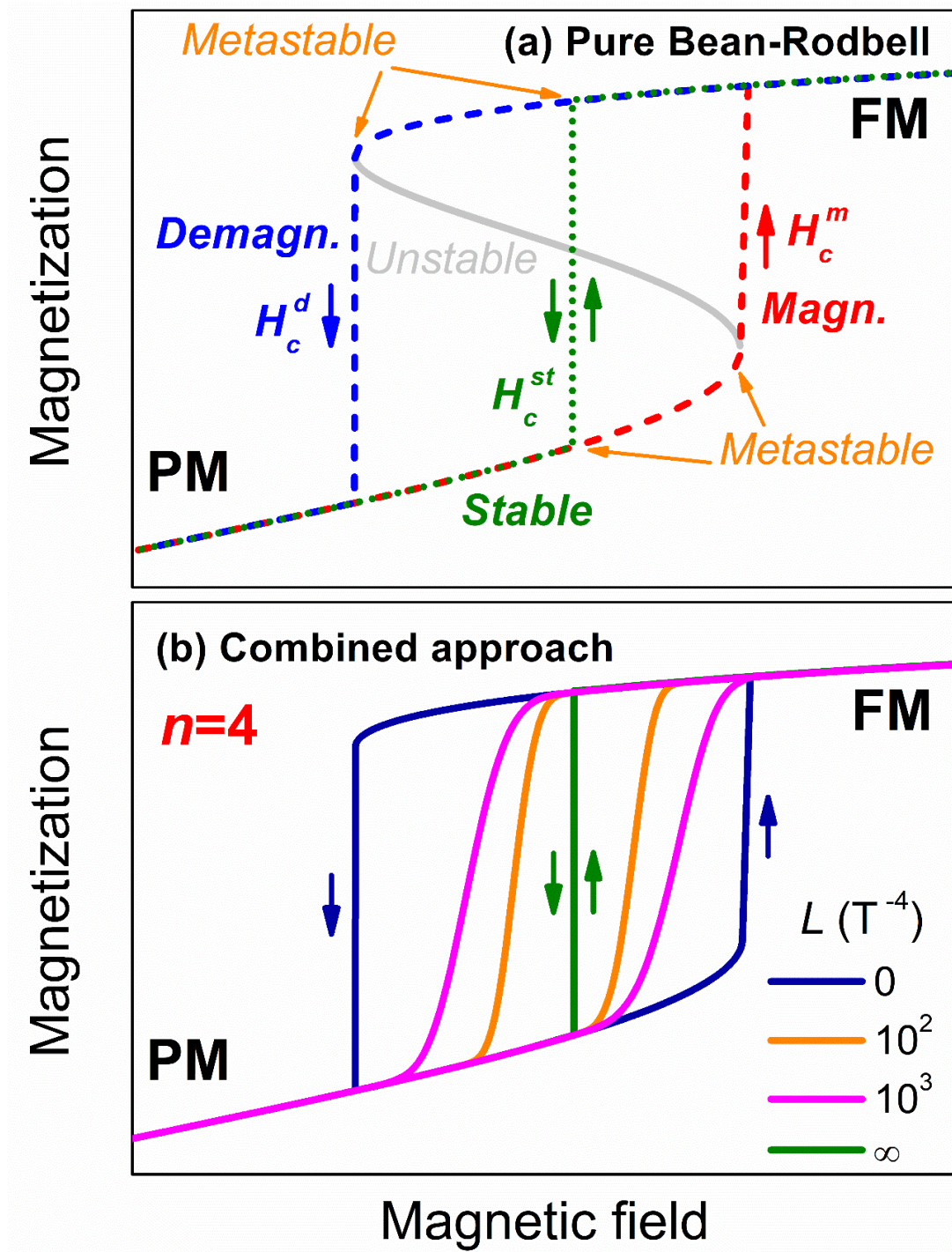| Temperature (K) | Process | $L$ ($T^{-4}$) | | $H_0$ (T) |
|---|---|---|---|---|
| 190 | Magnetization | 850(70) | | 0.632(4) |
| | Demagnetization | $X < 0.42$ | 45(4) | 0.685(5) |
| | | $X > 0.42$ | 460(30) | 0.554(3) |
| 192 | Magnetization | 1040(70) | | 1.044(3) |
| | Demagnetization | $X < 0.39$ | 64(5) | 1.111(5) |
| | | $X > 0.39$ | 540(60) | 0.985(6) |
| 194 | Magnetization | 930(40) | | 1.462(1) |
| | Demagnetization | $X < 0.35$ | 46(2) | 1.532(3) |
| | | $X > 0.35$ | 1040(130) | 1.408(5) |

**Figures**



**Fig 1.** Illustration of the pure Bean-Rodbell model (a) and the proposed combined kinetic and Bean-Rodbell approach (b).
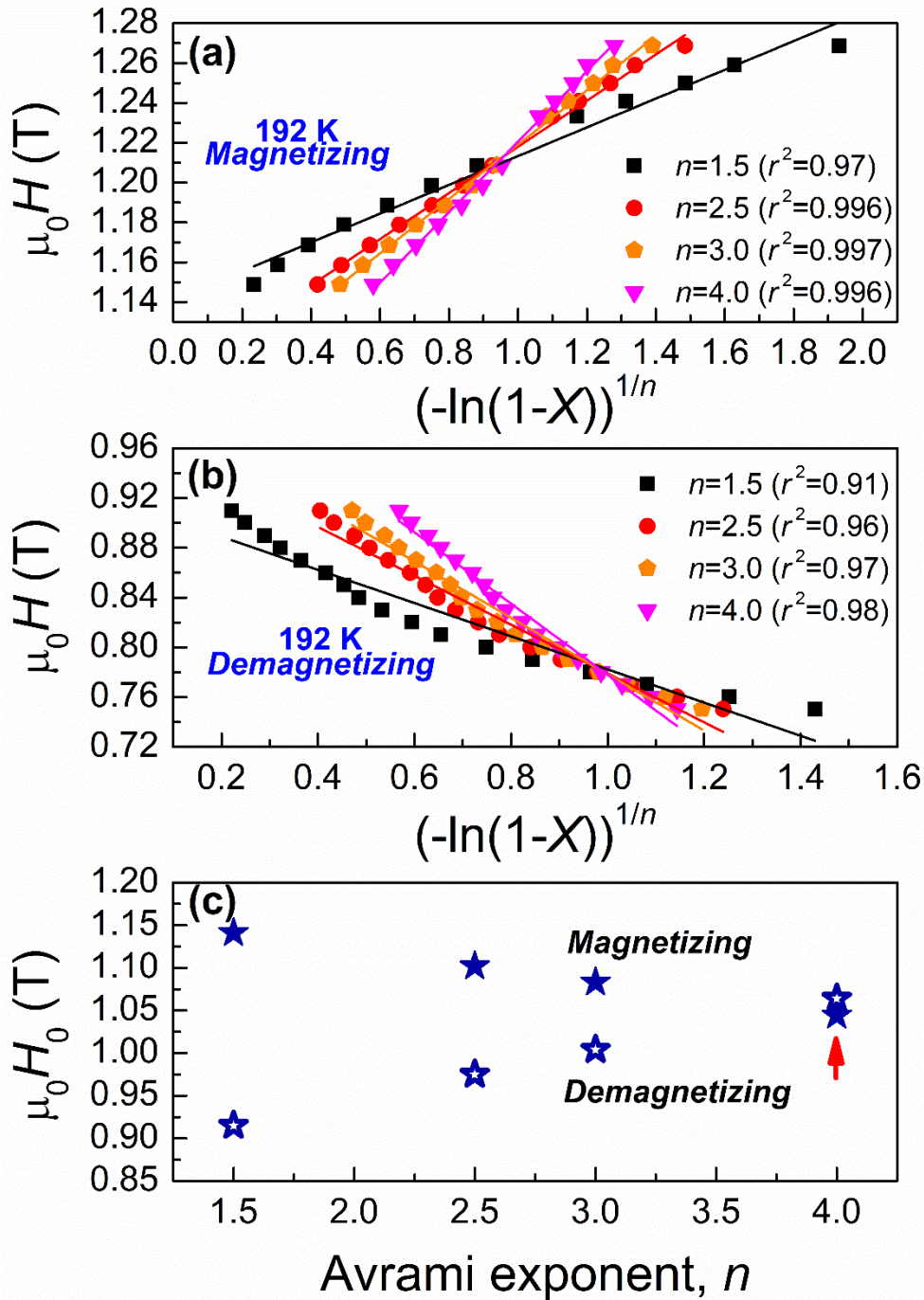
**Fig 2.** $H$ vs. $(-\ln(1-X))^{1/n}$ for different values of the Avrami exponent during the magnetization (a) and demagnetization (b) processes for the suction casted LaFe$_{11.6}$Si$_{1.4}$ sample at 50 Oe/s. (c) $H_0$ as a function of the Avrami exponents used (error bars are smaller than the symbol syze).
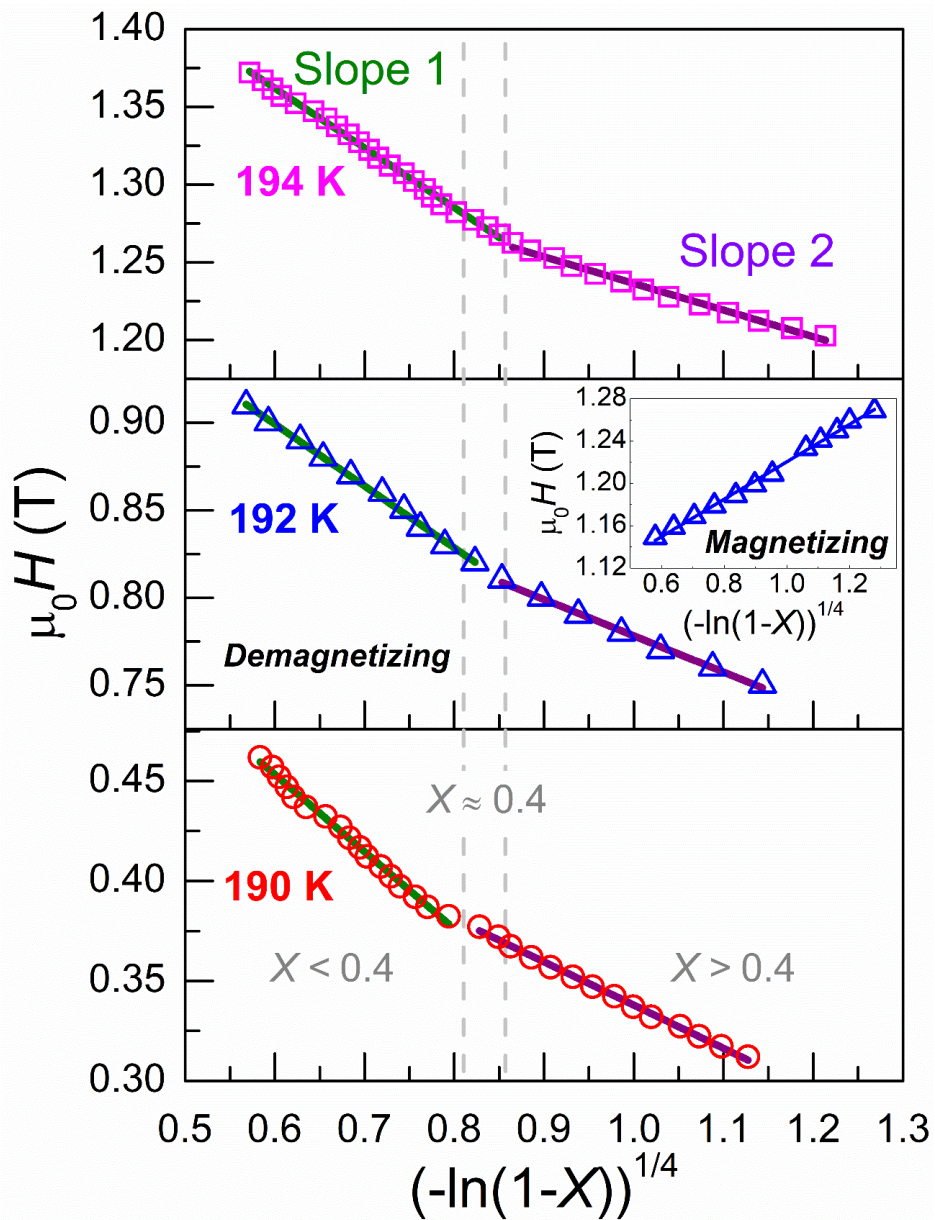
**Fig 3.** $H$ vs. $(-\ln(1-X))^{1/4}$ for the demagnetization curves at the three studied temperatures showing the two slope fitting for the suction casted $LaFe_{11.6}Si_{1.4}$ sample at 50 Oe/s. **Inset:** $H$ vs. $(-\ln(1-X))^{1/4}$ at 192 K for the magnetization curve.
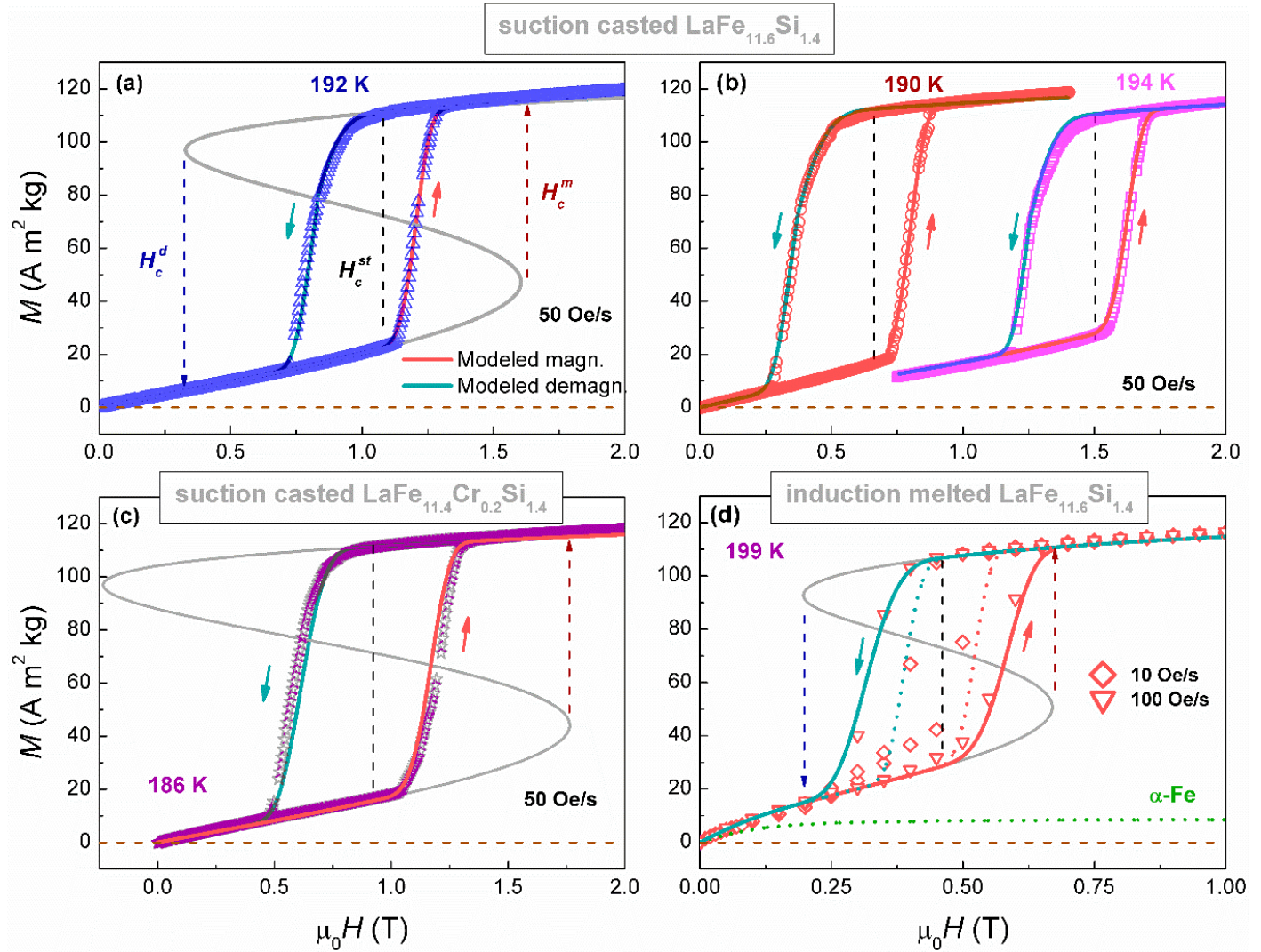
**Fig 4.** Experimental (symbols) and modeled (lines) magnetization and demagnetization processes at 192 K together with the pure Bean-Rodbell model without kinetic effects (a) and for the rest of studied temperatures (190 and 194 K) (b) for the suction casted LaFe$_{11.6}$Si$_{1.4}$ sample at 50 Oe/s. The same comparison for the suction casted LaFe$_{11.4}$Cr$_{0.2}$Si$_{1.4}$ sample at 50 Oe/s (c) and the induction melted LaFe$_{11.6}$Si$_{1.4}$ sample at 10 Oe/s and 100 Oe/s (d). For interpretation of the color legend, the reader is referred to the electronic version of this article.

## References

1.      V. K. Pecharsky and K. A. Gschneidner, Phys. Rev. Lett. **78** (23), 4494-4497 (1997).
2.      V. Franco, J. S. Blázquez, J. J. Ipus, J. Y. Law, L. M. Moreno-Ramírez and A. Conde, Prog. Mater. Sci. **93**, 112-232 (2018).
3.      F. Guillou, H. Yibole, G. Porcari, L. Zhang, N. H. van Dijk and E. Brück, J. Appl. Phys. **116** (6), 063903 (2014).
4.      B. Kaeswurm, V. Franco, K. P. Skokov and O. Gutfleisch, J. Magn. Magn. Mater. **406**, 259-265 (2016).
5.      A. Fujita, S. Fujieda, Y. Hasegawa and K. Fukamichi, Phys. Rev. B **67** (10), 104416 (2003).
6.      I. A. Radulov, D. Y. Karpenkov, K. P. Skokov, A. Y. Karpenkov, T. Braun, V. Brabänder, T. Gottschall, M. Pabst, B. Stoll and O. Gutfleisch, Acta Mater. **127**, 389-399 (2017).
7.      T. Gottschall, K. P. Skokov, M. Fries, A. Taubel, I. Radulov, F. Scheibel, D. Benke, S. Riegg and O. Gutfleisch, Adv. Energy Mater. **9** (34), 1901322 (2019).
8.      O. Gutfleisch, T. Gottschall, M. Fries, D. Benke, I. Radulov, K. P. Skokov, H. Wende, M. Gruner, M. Acet, P. Entel and M. Farle, Philos. Trans. A Math. Phys. Eng. Sci. **374** (2074), 20150308 (2016).
9.      V. Provenzano, A. J. Shapiro and R. D. Shull, Nature **429** (6994), 853-857 (2004).
10.     J. D. Moore, K. Morrison, K. G. Sandeman, M. Katter and L. F. Cohen, Appl. Phys. Lett. **95** (25), 252504 (2009).
11.     J. Liu, T. Gottschall, K. P. Skokov, J. D. Moore and O. Gutfleisch, Nat. Mater. **11** (7), 620-626 (2012).
12.     Y. Liu, L. C. Phillips, R. Mattana, M. Bibes, A. Barthélémy and B. Dkhil, Nat. Commun. **7** (1), 11614 (2016).
13.     V. Basso, M. Piazzi, C. Bennati and C. Curcio, Phys. Status Solidi B **255** (2), 1700278 (2018).
14.     V. Basso, C. P. Sasso and M. LoBue, J. Magn. Magn. Mater. **316** (2), 262-268 (2007).
15.     C. P. Bean and D. S. Rodbell, Phys. Rev. **126** (1), 104-115 (1962).
16.     M. Piazzi, C. Bennati, C. Curcio, M. Kuepferling and V. Basso, Journal of Magnetism and Magnetic Materials **400**, 349-355 (2016).
17.     D. Y. Karpenkov, A. Y. Karpenkov, K. P. Skokov, I. A. Radulov, M. Zheleznyi, T. Faske and O. Gutfleisch, Phys. Rev. Appl. **13**, 034014 (2020).
18.     K. Motizuki, H. Ido, T. Itoh and M. Morifuji, *Electronic Structure and Magnetism of 3d-Transition Metal Pnictides*. (Springer-Verlag Berlin Heidelberg, 2010).
19.     J. S. Amaral and V. S. Amaral, Phys. Status Solidi A **211** (5), 971-974 (2014).
20.     H. N. Bez, K. K. Nielsen, P. Norby, A. Smith and C. R. H. Bahl, AIP Adv. **6** (5), 056217 (2016).
21.     G. F. Wang, *Magnetic and calorimetric study of magnetocaloric effect in intermetallics exhibiting first-order magnetostructural transitions*. (Universidad de Zaragoza, Zaragoza, 2012).
22.     E. Lovell, A. M. Pereira, A. D. Caplin, J. Lyubina and L. F. Cohen, Advanced Energy Materials **5** (6), 1401639 (2015).
23.     A. Waske, E. Lovell, A. Funk, K. Sellschopp, A. Rack, L. Giebeler, P. F. Gostin, S. Fähler and L. F. Cohen, APL Materials **4** (10), 106101 (2016).
24.     W. Brey, G. Nellis and S. Klein, International Journal of Refrigeration **47**, 85-97 (2014).
25.     A. N. Kolmogorov, Bull. Acad. Sci. USSR Phys. Ser. Math. **1**, 355-359 (1937).
26.     W. A. Johnson and R. F. Mehl, Trans. Am. Inst. Min. Met. Eng. **135**, 416-442 (1939).
27.     M. Avrami, J. Chem. Phys. **7**, 1103-1112 (1939).
28.     M. Avrami, J. Chem. Phys. **8**, 212-224 (1940).
29.     M. Avrami, J. Chem. Phys. **9**, 177-184 (1941).
30.     C. Romero-Muñiz, V. Franco and A. Conde, Phys. Chem. Chem. Phys. **19** (5), 3582-3595 (2017).
31.     J. Amaral, S. Das and V. Amaral, in *Thermodynamics*, edited by J. C. Moreno-Piraján (IntechOpen, Rijeka, 2011), pp. 173-198.

32.     H. B. Callen, *Thermodynamics and an introduction to thermostatistics*, 2nd ed. (John Wiley and Sons, New York, 1985).
33.     A. Fujita and H. Yako, J. Alloys Compd. **577**, S48-S51 (2013).
34.     H. Yako, S. Fujieda, A. Fujita and K. Fukamichi, IEEE Trans. Magn. **47** (10), 2482-2485 (2011).
35.     H. W. Zhang, F. Wang, T. Y. Zhao, S. Y. Zhang, J. R. Sun and B. G. Shen, Physical Review B **70** (21), 212402 (2004).
36.     J. Burke, *The Kinetics of Phase Transformations in Metals*. (Pergamon Press, Oxford, 1965).
37.     L. M. Moreno-Ramírez, C. Romero-Muñiz, J. Y. Law, V. Franco, A. Conde, I. A. Radulov, F. Maccari, K. P. Skokov and O. Gutfleisch, Acta Mater. **175**, 406-414 (2019).
38.     J. M. D. Coey, *Magnetism and Magnetic Materials*. (Cambridge University Press, Cambridge, 2010).
39.     J. W. Christian, *The Theory of Transformations in Metals and Alloys*, 3rd ed. (Pergamon, Oxford, 2002).
40.     L. Jia, J. R. Sun, H. W. Zhang, F. X. Hu, C. Dong and B. G. Shen, J. Phys.: Condens. Matter **18** (44), 9999-10007 (2006).